IEEE Access
Multidisciplinary ⋮ Rapid Review ⋮ Open Access Journal

Received May 26, 2020, accepted June 2, 2020, date of publication June 5, 2020, date of current version June 17, 2020.

Digital Object Identifier 10.1109/ACCESS.2020.3000309

New Double Closed Loop Linear Active Disturbance Rejection Control of Energy Storage Grid-Connected Inverter Based on Lead-Lag Correction Link

YOUJIE MA, LUYONG YANG, XUESONG ZHOU, AND XIA YANG

Tianjin Key Laboratory for Control Theory and Applications in Complicated Industry Systems, School of Electrical and Electronic Engineering, Tianjin University of Technology, Tianjin 300384, China

Corresponding authors: Luyong Yang (183125317@stud.tjut.edu.cn) and Xuesong Zhou (zxsmyj@126.com)

This work was supported in part by the National Natural Science Foundation of China under Grant 51877152, and in part by the Natural Science Foundation of Tianjin of China under Grant 18JCZDJC97300.

ABSTRACT The energy storage grid-connected inverter system is a complex system with strong nonlinearity and strong coupling, which quality and efficiency of grid-connection are affected by factors such as grid voltage fluctuations and model uncertainty. Based on the analysis of the working principle of the grid-connected energy storage system, this paper aims to improve the performance of the traditional linear active disturbance rejection control (LADRC) technology, in order to overcome the problems of serious phase lag of linear extended state observer (LESO) and poor ability to suppress high-frequency noise on the basis of introducing the proportional differential link in the traditional LESO, the differential term of output voltage error is introduced in LESO. In addition, the output of the channel for total disturbance is corrected to improve the disturbance observation ability of LESO against high-frequency noise. The theoretical proof of LADRC and the comparative analysis of Bode plots show that the improved LADRC has better anti-interference performance. Finally, to verify the effectiveness of the control strategy designed in this paper, different types of low-voltage ride-through faults are designed on the grid-side. The simulation results show that the new controller can improve the control performance effectively of the energy storage grid-connected system.

INDEX TERMS Energy storage grid-connected inverter system, linear active disturbance rejection control, linear extended state observer, proportional differential link, link correction, high frequency disturbance observation.

I. INTRODUCTION

Energy is the material basis for the survival and development of human society, and how to develop and utilize renewable energy reasonably is the embodiment of the degree of progress of human society. At the same time, which also opens up a new way to solve the energy crisis of the whole world. Increasing energy shortages and environmental pollution problems have caused new energy to be valued and applied widely [1], [2]. At this stage, with the continuous access of wind power generation system and photo-voltaic power generation system, the grid connection of energy storage system is becoming the research hot spot currently [3], [4]. In energy storage grid-connected systems, the design of grid-connected inverters is the core of the entire system control, and which is also a power electronic converter that realizes DC-AC conversion [5], [6].

The energy storage inverter system adopts the voltage and current double loop control of proportional integral (PI) regulator generally, which has the advantages of simple control structure and easy to realize. However, the traditional PI double loop control is difficult to achieve the ideal control effect in the situation of multivariable, strong coupling, strong nonlinearity and system parameter perturbation. Therefore, researcher Han Jingqing of the Chinese Academy of Sciences proposed the concept of active disturbance rejection control (ADRC) on the basis of the nonlinear proportional integral differential(PID)controller. The ADRC designed

The associate editor coordinating the review of this manuscript and approving it for publication was Shihong Ding.

accordingly does not depend on the precise mathematical model of the controlled object, and which simplifies the control system design greatly. The principle of ADRC is to take the uncertainty of the object model, external disturbances and real-time changes of parameters as a total disturbance, to observe and compensate it in real time [7]–[9]. At present, the control technology has been used widely. For example, in terms of disturbance observers, in [10], a design method of disturbance observer (DOB) for a class of nonlinear systems described by input-output differential equations is proposed, and which convergence is proved by mathematical analysis. This method has been applied to the disturbance estimation of nonlinear systems successfully, and a new linear DOB form has been developed. Reference [11] proposes an estimation method of induction motor speed regulation based on active disturbance rejection observer (ADRO) to achieve sensorless control of induction motors, which can estimate external disturbances in real time.

The traditional nonlinear ADRC contains too many parameters and it is difficult to adjust. Most of the research on this method in the control system design is still in the simulation stage or through the empirical method to get the similar optimal control effect, there is not a set of perfect theoretical basis. To reduce the number of parameter tuning, Professor Gao Zhiqiang, a famous American scholar, has designed the structures of ADRC by linearization, and proposed a linear ADRC method [12]. In this method, the concept of bandwidth is introduced into ADRC, and the controller parameters are related to the controller bandwidth and observer bandwidth. The algorithm is simple and easy to implement in engineering, which reduces the difficulty of debugging greatly. ESO is the core link that affects the performance of ADRC technology, and research on ESO has always been an important topic. In [13], a novel initial fault estimation scheme based on descriptor observer is designed, which is used for the initial fault evaluation of high-speed railway traction equipment, and the result is very good; Reference [14] proposes a novel robust diagnostic design scheme to observe the failure of the initial stator / rotor winding failure; Reference [15] for the reliable design of takagi sugeno multiple integral unknown input observer (TSMIUIO), a nonlinear system affected by time-varying actuator and sensor faults at the same time, the robust fault reconstruction is realized by using ESO to estimate the two-way interaction of actuator and sensor faults at the same time, which improves the control effect of the system greatly. Reference [16] from the frequency domain point of view, through mathematical derivation and Bode plot simulation analysis LESO has a good dynamic tracking estimation ability and filtering characteristics; In [17], a switching strategy between nonlinear and linear ESO is proposed, which combines the advantages of high tracking accuracy, fast response speed, convenient parameter setting of LESO and insensitivity to the variation of disturbance amplitude.

In order to further improve the control performance of traditional LADRC technology, on the basis of introducing the proportional differential link in the traditional LESO, to overcome the shortcomings of the serious phase lag of LESO and the problem of poor high-frequency noise suppression, an improved first-order LADRC with the output voltage and its differential as state variables is proposed to replace the voltage outer-loop controller in the traditional double-closed-loop control to construct a new double-closed-loop control strategy. Secondly, considering that LESO is the core link that affects LADRC control performance, the output voltage error differential term is introduced in LESO, and the first-order inertia link is added to the channel for the total disturbance to avoid the introduction of noise due to the increase of the observation bandwidth, thereby improving the anti-high frequency disturbance observation ability of LESO. Then, through frequency domain theoretical analysis and Bode plot simulation research, the LADRC before and after the improvement is compared and analyzed from the aspects of dynamic process and anti-interference ability, and the stability conditions of the improved LADRC under various conditions are given. Finally, taking the control of the super capacitor energy storage grid-connected inverter as the research object, a simulation model of the super capacitor energy storage system is established, and the low-voltage ride-through faults of different types and different degrees are designed on the grid-side [18], the effectiveness of the controller designed in this paper is verified by digital comparison simulation.

II. MATHEMATICAL MODELING OF ENERGY STORAGE CONVERSION SYSTEM AND GRID-SIDE INVERTER

A. ENERGY STORAGE CONVERSION SYSTEM

The super capacitor energy storage two-stage grid-connected structure is shown in Fig. 1, which is composed of super capacitor bank, power decoupling capacitor, DC / DC converter, three-phase inverter, three-phase filter and power grid. The focus of this article is to control the grid-connected

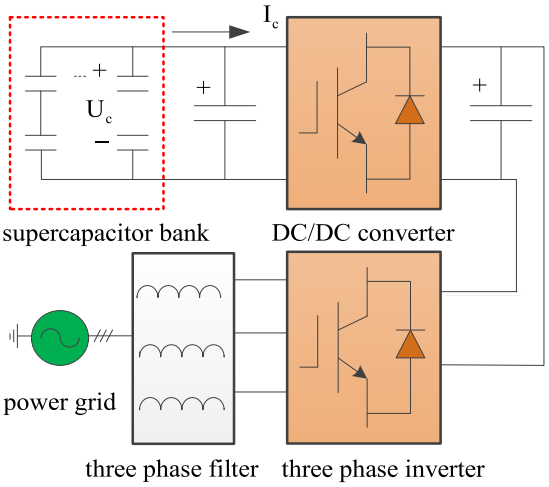

FIGURE 1. Super capacitor energy storage two-stage grid-connected structure.

inverter of the energy storage conversion system, so as to obtain a better steady-state performance of the DC-side bus voltage under grid-side faults. DC / DC converters usually use Boost boost circuits to convert the lower DC voltage of the super capacitor bank into a stable and higher DC voltage, which can meet the requirements of the grid-side inverter on the DC-side voltage amplitude. The DC / DC converter on the system side is mainly to change the output DC of the energy storage system into a stable DC, while ensuring a high power factor. The grid-side DC/AC converter realizes the function of stabilizing the DC bus voltage mainly, and at the same time converts the stable DC into a three-phase symmetrical sinusoidal AC, so as to facilitate the stable grid connection of the system. The two-stage energy storage grid-connected structure is more used commonly, and the circuit is simple and the technology is mature.The control objectives of each structure are clear, which is easy to meet the requirements of the system grid-connected.

B. MATHEMATICAL MODELING OF GRID-SIDE INVERTERS IN ENERGY STORAGE SYSTEM

The control structure of the grid-side inverter of the energy storage system is shown in Fig. 2. Where R, L, and C are the internal resistance of the filter inductor, filter inductor, and filter capacitor respectively; U_{sabc} is the three-phase voltage on the inverter side and the output side, and I_{sabc} is the three-phase current output.

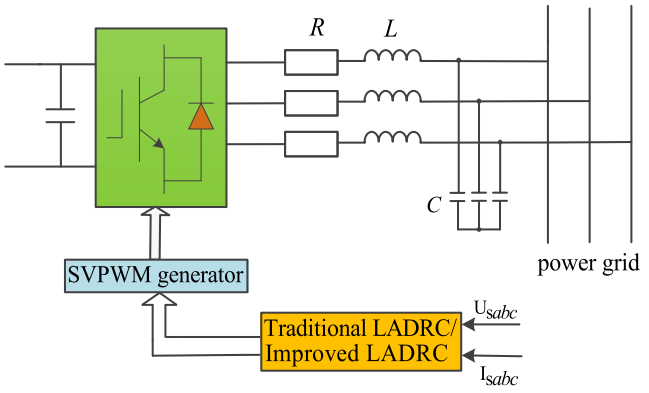

FIGURE 2. Control structure of grid-side inverter.

After the voltage equation of grid-side inverter is transformed by *Park*, the voltage equation of grid-side inverter in synchronous rotation coordinate system dq will be obtained [19]:

$$\begin{bmatrix} u_{gd} \\ u_{gq} \end{bmatrix} = R\begin{bmatrix} i_d \\ i_q \end{bmatrix} + L\begin{bmatrix} \frac{di_d}{d_t} \\ \frac{di_q}{d_t} \end{bmatrix} + \omega L\begin{bmatrix} -i_q \\ i_d \end{bmatrix} + \begin{bmatrix} u_d \\ u_q \end{bmatrix} \quad (1)$$

In equation(1), where u_{gd} and u_{gq} represent the components of grid voltage on axis dq respectively; i_d and i_q represent the components of the grid current on the dq-axis; u_d and u_q represent the components of the inverter output voltage on the dq-axis. If the phasor is three-phase symmetrical, the projection on axis d is E_s, and the projection on axis q is 0, then the output voltage $u_{gd} = E_s$, $u_{gq} = 0$, E_s is the amplitude of phase voltage of grid-side grid-connected inverter. Therefore, the equation (1) can be simplified as follows:

$$\begin{cases} u_d = -\left(Ri_d + L\dfrac{di_d}{dt}\right) + \omega Li_q + E_s \\ u_q = -\left(Ri_q + L\dfrac{di_q}{dt}\right) - \omega Li_d \end{cases} \quad (2)$$

If the reference voltage and power are selected, and the system parameter adopts the unit value, the instantaneous output power of grid-connected inverter [20] can be obtained:

$$\begin{cases} P = u_d i_d + u_q i_q = E_s i_d \\ Q = u_q i_d - u_d i_q = -E_s i_q \end{cases} \quad (3)$$

According to equation (3), which can be found that the active power and reactive power realize decoupling control, and then the power factor can be adjusted. The control block diagram of energy storage grid-connected inverter can be designed as shown in Fig. 3. The control of grid-connected inverter is a double closed-loop control strategy, and the external loop is an ADRC strategy to control the DC side bus voltage, so as to realize the stability of DC bus voltage. The internal loop is a PI control strategy to control the current, which can realize the unit power factor control when the energy storage system operates stably and increase the reactive power output when the inverter works in static synchronous compensator (STATCOM) mode when the grid-side fails.

When the system runs stably, the reference voltage u_{dc-ref} of the DC bus of the voltage control loop is compared with the actual voltage u_{dc} to obtain the active current reference value $i_{dc-ref1}$ after the LADRC regulator link, and the reactive current reference value i_{q-ref} is given as 0. In the current inner loop, the d and q axis current reference values are compared with the actual values i_d and i_q, respectively, and then pass through the PI regulator link, plus the coupling items ωLi_q, ωLi_d and d, q axis actual voltage values u_d and u_q to obtain voltage control the quantity u_{gd}, u_{gq}. Finally, the control value of the output three-phase voltage is obtained by coordinate transformation.

When the grid voltage drops, the reactive current reference value i_{q-ref} in the voltage outer loop is determined by the voltage drop depth, that is, the actual value of the grid voltage E_s is compared with the reference value E_{s-ref} through the PI link, and the active reference current is obtained according to equation $i_{dc-ref2} = \sqrt{i_{\max}^2 - i_{q-ref}^2}$ (Where $i_{\max}$ is the maximum current allowed by the converter), at the same time, the protection circuit on the DC side can be activated selectively, and the current inner loop control is unchanged, thereby the reactive power output by the inverter is increased, and the voltage at the grid-side is restored, so as to maintain the stable operation of the system.

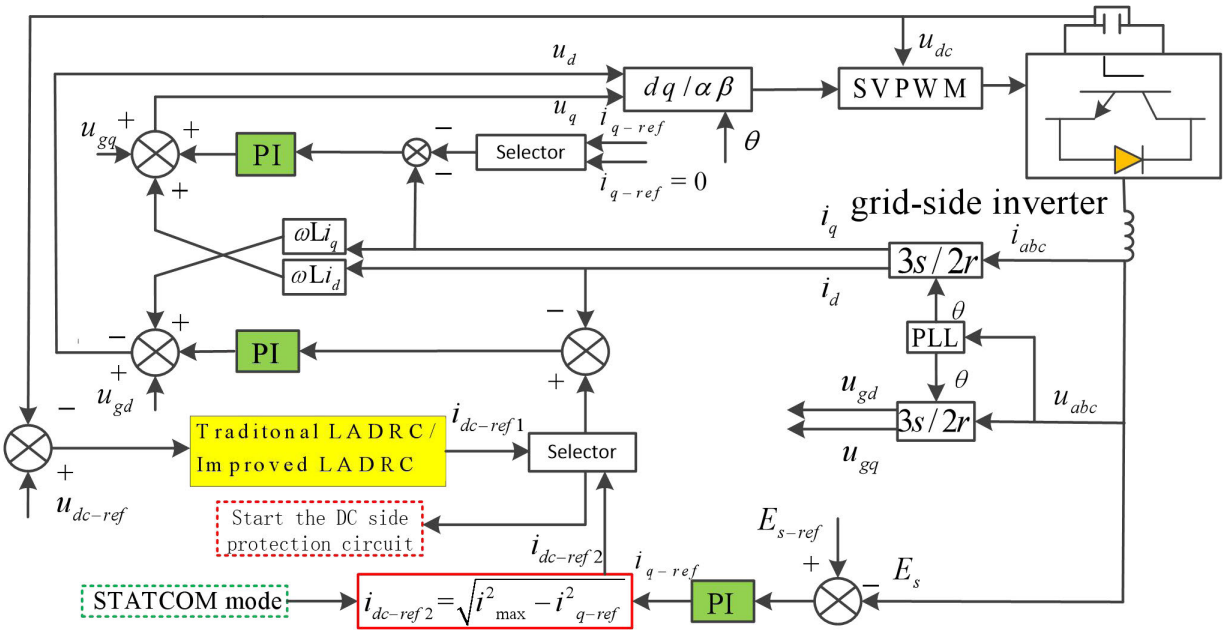

FIGURE 3. Control structure of energy storage grid-connected inverter.

III. THEORETICAL ANALYSIS OF TRADITIONAL FIRST-ORDER LADRC

A. THEORETICAL ANALYSIS OF TRADITIONAL SECOND-ORDER LESO

LADRC can treat external disturbance, parameter uncertainty and coupling as sum disturbance, estimate and compensate by LESO, and compensate the system as pure integral series type. The differential equation can be described as follows:

$$\dot{y} = -a_0 y + w + bu \tag{4}$$

In equation (4), where u and y are the input and output of the system, w is the unknown disturbance, a_0 is the parameter of the system, b is the input control gain, b is unknown, and b_0 is the estimated value of b. Let $x_1 = y, f(y,w) = -a_0 y + w + (b - b_0)u$ be the generalized disturbance of the system, including all uncertain factors and unknown external disturbances. Let $x_2 = f(y,w), h = f(y,w)$, the state equation of the system will be:

$$\begin{bmatrix} \dot{x}_1 \\ \dot{x}_2 \\ y \end{bmatrix} = \begin{bmatrix} 0 & 1 \\ 0 & 0 \\ 1 & 0 \end{bmatrix} \begin{bmatrix} x_1 \\ x_2 \end{bmatrix} + \begin{bmatrix} b_0 & 0 \\ 0 & 1 \\ 0 & 0 \end{bmatrix} \begin{bmatrix} u \\ h \end{bmatrix} \tag{5}$$

A second order LESO will be established:

$$\begin{bmatrix} \dot{z}_1 \\ \dot{z}_2 \end{bmatrix} = \begin{bmatrix} -\beta_1 & 1 \\ -\beta_2 & 0 \end{bmatrix} \begin{bmatrix} z_1 \\ z_2 \end{bmatrix} + \begin{bmatrix} b_0 & \beta_1 \\ 0 & \beta_2 \end{bmatrix} \begin{bmatrix} u \\ y \end{bmatrix} \tag{6}$$

In equation (6), where z_1 is the tracking signal of y, z_2 is the tracking signal of total disturbance, and β_1, β_2 are the coefficient of observer.

The linear state error feedback (LSEF) law of the system can be designed as follows [21]:

$$u = \frac{-z_2 + u_0}{b_0} \tag{7}$$

Neglecting the estimation error of z_2 to $f(y,w)$, equation (5) can be simplified as an integral link:

$$\dot{y} = x_2 + b_0 u = x_2 + (-z_2 + u_0) \approx u_0 \tag{8}$$

Because the differential of the state is not observed, the LSEF control law adopts the following proportional control:

$$u_0 = k_p(v - z_1) \tag{9}$$

B. PARAMETER DESIGN OF TRADITIONAL FIRST-ORDER LADRC

According to the pole configuration, the pole of equation (6) is arranged on the bandwidth ω_0 of the observer:

$$\lambda(s) = s^2 + \beta_1 s + \beta_2 = (s + \omega_0)^2 \tag{10}$$

Then:

$$\beta_1 = 2\omega_0, \quad \beta_2 = \omega_0^2 \tag{11}$$

Similarly, according to [16] can obtain:

$$k_p = \omega_c \tag{12}$$

Therefore, LADRC can be simplified to control the bandwidth ω_0 of the system observer and the bandwidth ω_c of the controller, and a reasonable adjustment of these two parameters can obtain a better control effect. For the controller applied in this paper, during the parameter setting process,

the following principles can be used: selecting the initial values of parameters ω_c and ω_0, keeping ω_c unchanged, and increasing ω_0 gradually until the noise effect is difficult to meet the system requirements. Increasing ω_c gradually, when the impact of noise is unbearable, the system output fluctuations are reduced, and then ω_0 is increased gradually, and increasing ω_c gradually. Thereby, adjusting of parameters according to this cycle, until the control requirements are met. In the process of adjusting the parameters, b_0 can be adjusted properly when there is too much oscillation in the dynamic tracking process of the system, so as to achieve the expected control effect. Finally, according to the experience and simulation results, the parameters of voltage outer loop LADRC are selected as $\omega_c = 3000$ and $\omega_0 = 500$ to analyze the control effect of LADRC before and after the improvement.

IV. STRUCTURAL DESIGN AND PERFORMANCE ANALYSIS OF IMPROVED FIRST-ORDER LADRC

A. PRINCIPLE ANALYSIS OF IMPROVED SECOND-ORDER LESO

From equation (6), we can get the traditional second-order LESO disturbance observation transfer function:

$$\phi(s) = \frac{\beta_2}{s^2 + \beta_1 s + \beta_2} \tag{13}$$

$\phi(s)$ as a second-order system, which frequency characteristics are similar to those of a typical second-order system, and there is a contradiction between speediness and overshoot in the time domain; there are characteristics of phase lag and serious amplitude attenuation in the frequency domain, which determines that the disturbance observation performance of the traditional second-order LESO is not ideal. Therefore, we need to improve the traditional second-order LESO to enhance the control performance of LESO and improve its control effect on the system.

1) A NEW TYPE OF SECOND ORDER LESO WITH PROPORTIONAL AND DIFFERENTIAL LINKS

According to equation (13), $\phi(s)$ is a second-order system, so comparing with a standard second-order system shows:

$$w_n = \sqrt{\beta_2}, \quad \zeta = \frac{\beta_1}{2\sqrt{\beta_2}} \tag{14}$$

In equation (14), where w_n is the undamped natural oscillation angular frequency of the system, while ζ is the damping ratio of the system.

In a standard second-order system, the time response and frequency response depend primarily on w_n and ζ. It can be seen from equation (14) that changes in the two indexes w_n and ζ affect the changes in the two gains β_1 and β_2, and the change in the gain of β_2 can affect both w_n and ζ at the same time. Therefore, this paper proposes a new type of LESO by improving the observation gain coefficient β_2 of traditional LESO. The improved equation is as follows:

$$\beta_2(s) = \beta_a(1 + \beta_b s) \tag{15}$$

In equation (15), where β_a and β_b are proportional differential coefficients, respectively, and the improved β_2 includes the proportional differential link. At this time, the transfer function of disturbance observation can be expressed as:

$$\phi_{(s)} = \frac{\beta_a(1 + \beta_b s)}{s^2 + (\beta_1 + \beta_a\beta_b)s + \beta_a} \tag{16}$$

Compared with equation (13), the most obvious change of equation (16) is to increase a zero point, reduce the peak time, and speed up the response of the system. Connecting a leading network in series, reducing the slope of the amplitude decline, and improving the stability of the system.

It can be seen from Fig. 4 that increasing the bandwidth ω_0 can improve the disturbance observation ability of LESO, but affected by factors such as observation noise, with the continuous increase of frequency, the disturbance observation performance of traditional LESO is not very good. Therefore, this method has limited performance improvement for LESO.

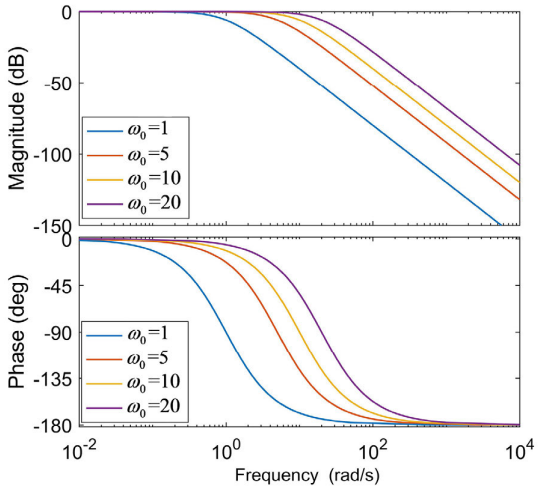

FIGURE 4. Frequency characteristics of traditional LESO disturbance transfer function.

It can be seen from Fig. 5 that the introduction of the new LESO with proportional differential not only increases the observation bandwidth of the system, but also compensates the phase lag. However, although the observation bandwidth of LESO is increased significantly by the above methods, the suppression ability of LESO against high frequency noise is also reduced. Therefore, the application of the new type of LESO does not improve the control performance effectively of the LESO to a certain extent. So, increasing the observation bandwidth of the LESO and solving the problem of the poor noise suppression ability of the LESO in the high frequency band, which is necessary to continue to optimize and improve the new type of LESO.

2) IMPROVED SECOND-ORDER LESO WITH LEADING AND LAGGING LINKS

Through the above analysis of the insufficient application of the new LESO, to ensure that it can increase the observation bandwidth effectively of LESO and solve the problem of poor suppression of LESO at high-frequency noise, referring to the

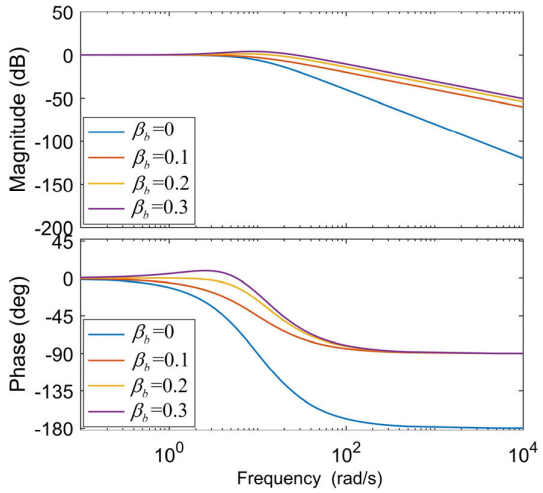

FIGURE 5. Frequency characteristics of a new LESO disturbance transfer function with proportional differentiation.

lead correction and lag correction in the automatic control principle method [22], which improve equation (15) to the following expression:

$$\beta_2' = \beta_2 \frac{T_\alpha s + 1}{\alpha T_\alpha s + 1} \tag{17}$$

In equation (17), T_α is the leading time constant; α is a coefficient between 0 and 1.

The improvement of equation (17) is equivalent to the observation gain coefficient of the total disturbance. On the basis of introducing the proportional differentiation link (leading link), to overcome the problems of serious LESO phase lag and poor high-frequency noise suppression, the channel for the total disturbance is used specially. The output is subjected to link correction (lagging link) to improve the anti-high frequency noise disturbance observation ability of LESO, thereby further optimizing the controller and improving the control performance of the system.

As shown in Fig. 6, compared to the new LESO, the improved LESO has almost the same bandwidth and phase characteristics in the low and middle frequency bands,

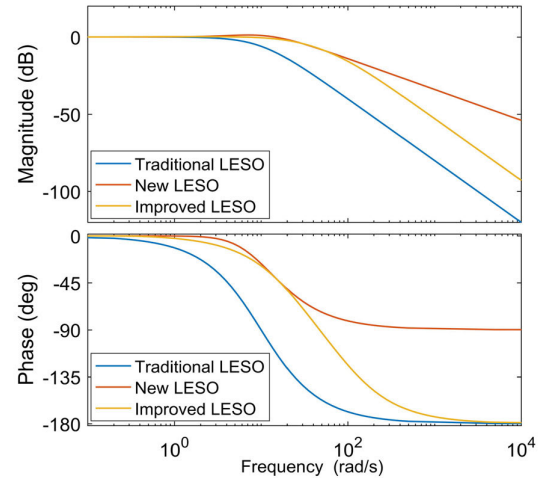

FIGURE 6. Comparison of three LESO disturbance estimation capabilities.

and the high frequency attenuation capability is enhanced significantly. For the improved LESO, which not only increases the observation bandwidth of LESO, but also improves the observation ability of the total disturbance of LESO at high frequency noise. Therefore, the improved LESO designed in this paper has more practical application value and can reach a certain control effect.

B. STRUCTURE DESIGN OF IMPROVED FIRST-ORDER LADRC

Through the analysis above, the state space equation for improving LESO can be written as follows:

$$\begin{bmatrix} \dot{z}_1 \\ \dot{z}_2 \\ \dot{z}_3 \end{bmatrix} = \begin{bmatrix} -\beta_1 & 1 & 0 \\ \beta_1\beta_2 T_\alpha - \beta_2 & -\beta_2 T_\alpha & 0 \\ 0 & \frac{1}{\alpha T_\alpha} & -\frac{1}{\alpha T_\alpha} \end{bmatrix} \begin{bmatrix} z_1 \\ z_2 \\ z_3 \end{bmatrix} + \begin{bmatrix} b_0 & \beta_1 & 0 \\ -\beta_2 T_\alpha b_0 & \beta_2 - \beta_1\beta_2 T_\alpha & \beta_2 T_\alpha \\ 0 & 0 & 0 \end{bmatrix} \begin{bmatrix} u \\ y \\ \dot{y} \end{bmatrix} \tag{18}$$

In equation (18), z_3 is the total disturbance that the improved LESO acts on the system finally, and which is obtained by z_2 correcting through the link of the total disturbance channel.

From equation (18), the transfer functions of z_1, z_2, and z_3 of the improved LADRC can be obtained as:

$$\begin{cases} z_1 = \dfrac{\left(\omega_0^2 T_\alpha + 2\omega_0\right) s + \omega_0^2}{s^2 + \left(\omega_0^2 T_\alpha + 2\omega_0\right) s + \omega_0^2} y \\ \quad + \dfrac{s}{s^2 + \left(\omega_0^2 T_\alpha + 2\omega_0\right) s + \omega_0^2} b_0 u \\ z_2 = \dfrac{\omega_0^2 T_\alpha s^2 + \omega_0^2 s}{s^2 + \left(\omega_0^2 T_\alpha + 2\omega_0\right) s + \omega_0^2} y \\ \quad - \dfrac{\omega_0^2 T_\alpha s + \omega_0^2}{s^2 + \left(\omega_0^2 T_\alpha + 2\omega_0\right) s + \omega_0^2} b_0 u \\ z_3 = \dfrac{1}{\alpha T_\alpha s + 1} z_2 \end{cases} \tag{19}$$

The control structure of LADRC can be improved by combining (9) and (18) as shown in Fig. 7:

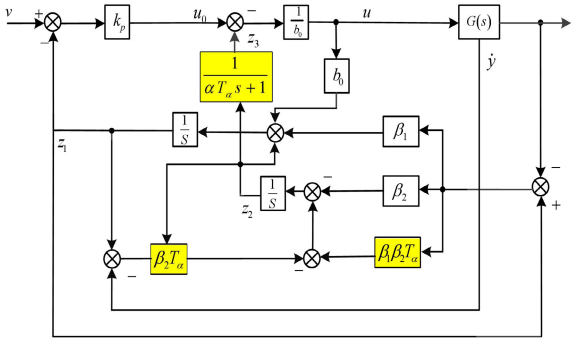

FIGURE 7. Improved LADRC control structure.

The control rate of the improved LADRC can be designed as:

$$u = \frac{-z_3 + u_0}{b_0} \tag{20}$$

After simplified calculation, the following equation can be obtained:

$$u = \frac{1}{b_0} G_1(s)\left[\omega_c v - G(s)\, y\right] \tag{21}$$

$G_1(s)$ and $H(s)$ are given in (21), shown at the bottom of this page.

According to equation (21), the simplified system structure diagram as shown in Fig. 8:

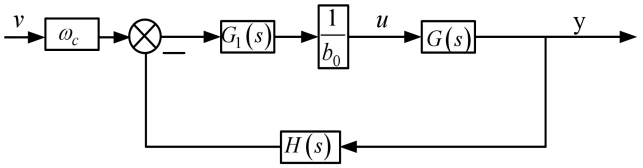

FIGURE 8. Simplified system structure diagram.

It can be seen from Fig. 8 that LADRC is a feedback system, and which essential problem is the stability of the system, while the essential problem of the control system is the anti-disturbance characteristic. This part uses the classical control theory method to analyze the anti-disturbance characteristics and stability mainly of the improved first-order LADRC in the frequency domain.

C. CONVERGENCE ANALYSIS OF IMPROVED SECOND-ORDER LESO

Improving LESO is the core of LADRC, which tracking and estimation ability is the key to affect the performance of LADRC, so we first analyze it.

According to equation (19), the tracking errors $e_1 = z_1 - y$, $e_2 = z_3 - f$ can be obtained as:

$$\begin{cases} e_1(s) = \dfrac{-s^2}{s^2 + (\omega_0^2 T_\alpha + 2\omega_0)s + \omega_0^2} y \\ \quad + \dfrac{s}{s^2 + (\omega_0^2 T_\alpha + 2\omega_0)s + \omega_0^2} b_0 u \\ e_2(s) = -\dfrac{\alpha T_\alpha s^4 + (\alpha T_\alpha^2 \omega_0^2 + 2\alpha T_\alpha \omega_0 + 1)s^3}{(\alpha T_\alpha s + 1)\left[s^2 + (\omega_0^2 T_\alpha + 2\omega_0)s + \omega_0^2\right]} y \\ \quad + \dfrac{(\alpha T_\alpha \omega_0^2 + 2\omega_0)s^2}{(\alpha T_\alpha s + 1)\left[s^2 + (\omega_0^2 T_\alpha + 2\omega_0)s + \omega_0^2\right]} y \\ \quad + \dfrac{\alpha T_\alpha s^3 + (\alpha T_\alpha^2 \omega_0^2 + 2\alpha T_\alpha \omega_0 + 1)s^2}{(\alpha T_\alpha s + 1)\left[s^2 + (\omega_0^2 T_\alpha + 2\omega_0)s + \omega_0^2\right]} b_0 u \\ \quad + \dfrac{(\alpha T_\alpha \omega_0^2 + 2\omega_0)s}{(\alpha T_\alpha s + 1)\left[s^2 + (\omega_0^2 T_\alpha + 2\omega_0)s + \omega_0^2\right]} b_0 u \end{cases} \tag{22}$$

For the convenience of analysis, both y and u take a step signal of amplitude K, that is, $y(s) = K/s$, $u(s) = K/s$ (K is a constant), and the steady-state error can be obtained:

$$\begin{cases} e(s) = \lim\limits_{s\to 0} s e_1(s) = 0 \\ e(s) = \lim\limits_{s\to 0} s e_2(s) = 0 \end{cases} \tag{23}$$

The equation (23) shows that the improved LESO has good convergence and estimation ability, and can realize the error-free estimation of system state variables and total disturbance.

D. ANALYSIS OF INTERFERENCE IMMUNITY TRACKING OF IMPROVED FIRST-ORDER LADRC

According to equation (8), the charged object can be:

$$y = \frac{1}{s}(f + b_0 u) \tag{24}$$

With reference to Fig.8, the closed-loop transfer function of the system will be:

$$G_{c1}(s) = \frac{\omega_c G_1(s)\, G(s)/b_0}{1 + G_1(s)\, G(s)\, H(s)/b_0} \tag{25}$$

Substituting $G_1(s)$, $G(s)$, and $H(s)$ will be obtained:

$$\begin{aligned} y = \frac{\omega_c}{s+\omega_c} v + \frac{\alpha T_\alpha s^3 + \left(\alpha T_\alpha \omega_0^2 + 2\omega_0 + \omega_c\right)s}{(\alpha T_\alpha s + 1)(s+\omega_c)\left[s^2 + (T_\alpha \omega_0^2 + 2\omega_0)s + \omega_0^2\right]} f \\ + \frac{\left(\alpha T_\alpha^2 \omega_0^2 + 2\alpha T_\alpha \omega_0 + \alpha T_\alpha \omega_c + 1\right)s^2}{(\alpha T_\alpha s + 1)(s + \omega_c)\left[s^2 + \left(T_\alpha \omega_0^2 + 2\omega_0\right)s + \omega_0^2\right]} f \end{aligned} \tag{26}$$

It can be seen from equation (26) that the output of the system consists of the tracking term and the disturbance term. When the estimation error of the total disturbance f pair of the system is ignored, the output only contains the tracking term term. At this time, the control performance of the system is only determined by ω_c, and has nothing to do with ω_0. The larger the ω_c, the faster the tracking speed, and there is no overshoot in the tracking process. By adjusting the controller bandwidth, observer bandwidth, and inertial link coefficients, which the tracking and anti-interference can be controlled well. For the improved LADRC, when the leading lag link coefficient is fixed, selecting $\omega_0 = 100$, $\omega_c = 0.1$, 1, 10, 100, and the frequency characteristic curve can be obtained as shown in Fig. 9. When takes $\omega_c = 100$, $\omega_0 = 0.1$, 1, 10, 100, and the frequency characteristic curve can be obtained as shown in Fig 10.

As can be seen from Fig. 9 and Fig.10 that increasing ω_c and ω_0 can reduce the disturbance gain and enhance the anti-interference ability of the system, which can explain that

$$G_1(s) = \frac{(\alpha T_\alpha s + 1)\left[s^2 + \left(T_\alpha \omega_0^2 + 2\omega_0\right)s + \omega_0^2\right]}{\alpha T_\alpha s^3 + \left(2\alpha T_\alpha \omega_0 + \alpha T_\alpha \omega_c + \alpha T_\alpha^2 \omega_0^2 + 1\right)s^2 + \left(2\omega_0 + \omega_c + \alpha T_\alpha \omega_0^2\right)s}$$

$$H(s) = \frac{\left(T_\alpha \omega_0^2 + 2\alpha T_\alpha \omega_0 \omega_c + \alpha T_\alpha^2 \omega_0^2 \omega_c\right)s^2}{(\alpha T_\alpha s + 1)\left[s^2 + \left(T_\alpha \omega_0^2 + 2\omega_0\right)s + \omega_0^2\right]} + \frac{\left(\omega_0^2 + 2\omega_0 \omega_c + T_\alpha \omega_0^2 \omega_c + \alpha T_\alpha \omega_0^2 \omega_c\right)s + \omega_0^2 \omega_c}{(\alpha T_\alpha s + 1)\left[s^2 + \left(T_\alpha \omega_0^2 + 2\omega_0\right)s + \omega_0^2\right]}$$

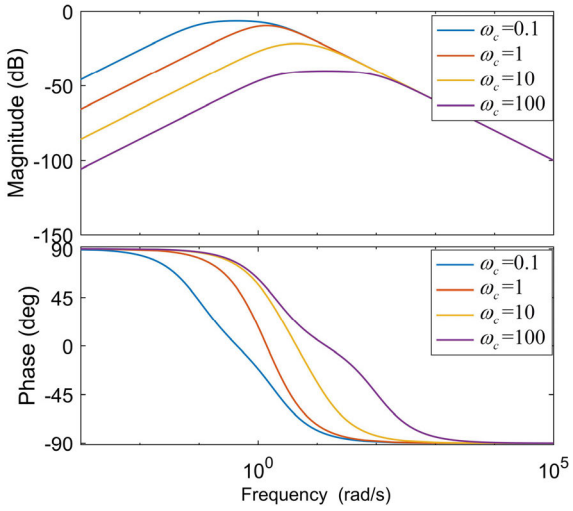

FIGURE 9. Disturbance frequency characteristic curve (ω_c change).

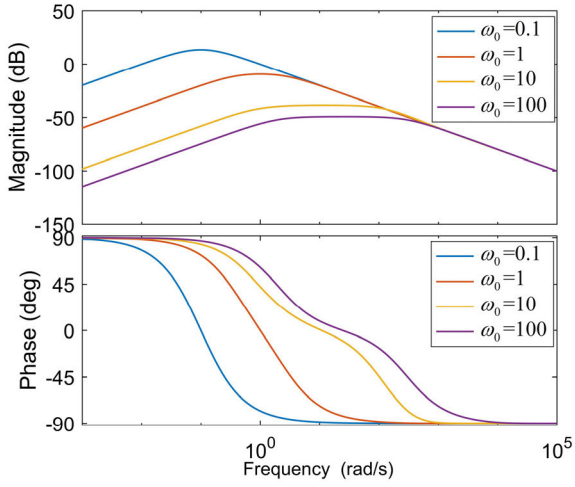

FIGURE 10. Disturbance frequency characteristic curve (ω_0 change).

the anti-disturbance performance of the improved LADRC is improved.

It can be seen from Fig. 11 that when $T_\alpha = 0$ is the disturbance characteristic curve of the traditional LADRC, and when the leading lag link coefficient is not 0, which is the disturbance characteristic curve of the improved LADRC. When the coefficient increases gradually, the anti-interference ability increases gradually of improved LADRC, which can show that the anti-interference performance of improved LADRC is superior to the traditional LADRC.

E. STABILITY ANALYSIS OF IMPROVED FIRST-ORDER LADRC IN ENERGY STORAGE SYSTEMS

1) STABILITY ANALYSIS OF IMPROVED FIRST-ORDER LADRC CONSIDERING THE UNCERTAINTY OF CONTROL INPUT GAIN

The influence of external disturbance and model parameter uncertainty is not considered temporarily, namely $f(t, y, w) = (b - b_0)\, u(t)$, Laplace transform is $F(s) = (b - b_0)\, U(s)$.

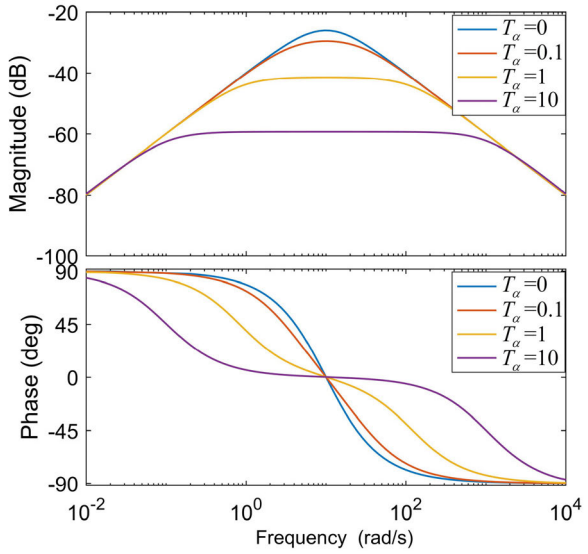

FIGURE 11. Analysis of the influence of the leading lag link coefficient on the anti-interference characteristics of LADRC.

Simultaneous (8) can be obtained:

$$y = \frac{1}{s}\left[(b - b_0)\, U(s) + b_0 U(s)\right] \tag{27}$$

According to equation (25), the closed-loop transfer function of the system will be:

$$y = \frac{(\alpha T_\alpha s + 1)\left[s^2 + \left(T_\alpha \omega_0^2 + 2\omega_0\right) s + \omega_0^2\right]\omega_c}{a_4 s^4 + a_3 s^3 + a_2 s^2 + a_1 s^1 + a_0} \tag{28}$$

In the equation (28):

$$\begin{aligned}
a_4 &= \alpha T_\alpha b_0 \\
a_3 &= b_0 + \alpha T_\alpha \omega_c b_0 + \alpha T_\alpha^2 \omega_0^2 b_0 + 2\alpha T_\alpha \omega_0 b_0 \\
a_2 &= \alpha T_\alpha^2 \omega_0^2 \omega_c + \alpha T_\alpha \omega_0^2 b_0 + 2\alpha T_\alpha \omega_c + \omega_c b_0 + 2\omega_0 b_0 \\
&\quad + T_\alpha \omega_0^2 \\
a_1 &= \omega_0^2 + 2\omega_0 \omega_c + T_\alpha \omega_0^2 \omega_c + \alpha T_\alpha \omega_0^2 \omega_c \\
a_0 &= \omega_0^2 \omega_c
\end{aligned}$$

Since the controller bandwidth ω_c and observer bandwidth ω_0 are both positive, which can be seen that $a_i > 0$ $(i = 0, 1, 2, 3, 4, 5)$.

From the Leonard-Chipat stability criterion, the sufficient and necessary condition for the energy storage grid-connected inverter system to remain stable is that its odd-order Horwitz determinant is positive, so the condition for improving the stability of the LADRC system is $\Delta_1 > 0, \Delta_3 > 0$.

$$\Delta_1 = a_1 > 0, \quad \Delta_3 = \begin{vmatrix} a_1 & a_0 & 0 \\ a_3 & a_2 & a_1 \\ 0 & a_4 & a_3 \end{vmatrix} > 0 \tag{29}$$

Therefore, the energy storage grid-connected inverter system remains stable.

2) STABILITY ANALYSIS OF IMPROVED FIRST-ORDER LADRC CONSIDERING THE UNCERTAINTY OF MODEL PARAMETERS

According to equation (8) and equation (18), the controlled object of the improved first-order LADRC can be recorded as:

$$y = \frac{b_0}{s + k_c} u \tag{30}$$

where k_c is an unknown parameter.

According to equation (25), the closed-loop transfer function of the system can be obtained as:

$$y = \frac{(\alpha T_\alpha s + 1)\left[s^2 + \left(T_\alpha \omega_0^2 + 2\omega_0\right) s + \omega_0^2\right] \omega_c}{d_4 s^4 + d_3 s^3 + d_2 s^2 + d_1 s^1 + d_0} \tag{31}$$

In the equation (31):

$$\begin{aligned}
d_4 &= \alpha T_\alpha b_0 \\
d_3 &= b_0 + \alpha T_\alpha \omega_c b_0 + \alpha T_\alpha^2 \omega_0^2 b_0 + 2\alpha T_\alpha \omega_0 b_0 + \alpha T_\alpha b_0 k_c \\
d_2 &= \alpha T_\alpha^2 \omega_0^2 \omega_c + \alpha T_\alpha \omega_0^2 b_0 + 2\alpha T_\alpha \omega_c \omega_0 + 2\omega_0 b_0 + T_\alpha \omega_0^2 \\
&\quad + \omega_c b_0 + k_c \left(\alpha T_\alpha \omega_c b_0 + \alpha T_\alpha^2 \omega_0^2 b_0 + 2\alpha T_\alpha \omega_0 b_0 + b_0\right) \\
d_1 &= \omega_0^2 + 2\omega_0 \omega_c + \alpha T_\alpha \omega_0^2 \omega_c + \alpha T_\alpha \omega_0^2 \omega_c \\
&\quad + k_c \left(2\omega_0 b_0 + \omega_c b_0 + \alpha T_\alpha \omega_0^2 b_0\right) \\
d_0 &= \omega_0^2 \omega_c
\end{aligned}$$

Similar to the previous section, the conditions for improving the stability of the LADRC system will be:

$$\Delta_3 = d_1 d_2 d_3 - d_1^2 d_4 - d_0 d_3^2 > 0 \tag{32}$$

As can be seen from equation (32) that which contains unknown number k_c compared to equation (25), so the system stability cannot be determined by the above method. If $k_c > 0$, the derivation from the previous section shows that the improved LADRC system remains stable. If $k_c < 0$, then equation (32) can be reduced to a third-order equation with k_c as the unknown, as follows:

$$c_3 k_c^3 + c_2 k_c^2 + c_1 k_c + c_0 > 0 \tag{33}$$

In the equation (33):

$$\begin{aligned}
c_3 &= h_2 h_4 h_6 \\
c_2 &= h_2 h_4 h_5 + h_1 h_4 h_6 + h_2 h_3 h_6 - h_2^2 b_4 - h_6^2 d_0 \\
c_1 &= h_1 h_4 h_5 + h_2 h_3 h_5 + h_1 h_3 h_6 - 2h_1 h_2 b_4 - 2h_5 h_6 d_0 \\
c_0 &= h_1 h_3 h_5 - h_1^2 b_4 - h_6^2 d_0 \\
h_1 &= \omega_0^2 + 2\omega_0 \omega_c + \alpha T_\alpha \omega_0^2 \omega_c + \alpha T_\alpha \omega_0^2 \omega_c \\
h_2 &= 2\omega_0 b_0 + \omega_c b_0 + \alpha T_\alpha \omega_0^2 b_0 \\
h_3 &= \alpha T_\alpha^2 \omega_0^2 \omega_c + \alpha T_\alpha \omega_0^2 b_0 + 2\alpha T_\alpha \omega_c \omega_0 + 2\omega_0 b_0 \\
&\quad + T_\alpha \omega_0^2 + \omega_c b_0 \\
h_4 &= \alpha T_\alpha \omega_c b_0 + \alpha T_\alpha^2 \omega_0^2 b_0 + 2\alpha T_\alpha \omega_0 b_0 + b_0 \\
h_5 &= b_0 + \alpha T_\alpha \omega_c b_0 + \alpha T_\alpha^2 \omega_0^2 b_0 + 2\alpha T_\alpha \omega_0 b_0 \\
h_6 &= \alpha T_\alpha b_0
\end{aligned}$$

Assuming that the roots of equation (33) corresponding to the equations are k_{c1}, k_{c2}, k_{c3}, and there is $k_{c1} < k_{c2} < k_{c3}$, then at $k_c < 0$, if the value of k_c satisfies $k_{c1} < k_c < k_{c2}$ or $k_c > k_{c3}$, the system remains stable.

In summary, the improved first-order LADRC system remains stable.

V. APPLICATION OF IMPROVED FIRST-ORDER LADRC IN SUPER CAPACITOR ENERGY STORAGE GRID-CONNECTED INVERTER SYSTEM

The super capacitor energy storage grid-connected system studied in this paper adopts double closed-loop control strategy, that is, the inner loop current loop adopts the traditional PI control strategy, and the outer loop voltage loop adopts the improved LADRC control strategy to ensure the stable output of the DC side bus voltage. Therefore, compared with the traditional PI double closed-loop control strategy, a new double closed-loop control strategy is proposed to improve the control performance of grid-connected inverter system in this paper.

A. DESIGN OF CURRENT LOOP STRUCTURE IN ENERGY STORAGE GRID-CONNECTED INVERTER SYSTEM

The control goal of the current loop is used to realize the stable output mainly of the grid-connected current. The design of this paper focuses on the control of the DC-side bus voltage of the outer loop voltage loop, and does not analyze the control effect of the inner loop current loop. The design of the current loop in this paper still uses the traditional PI control strategy. The control block diagram is shown in the following Fig. 12:

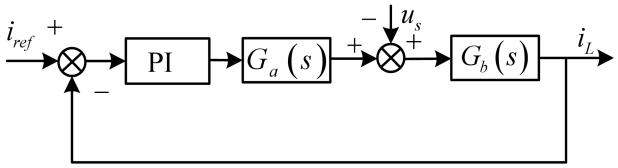

FIGURE 12. Schematic diagram of current loop control.

Among them, i_{ref} is the control reference input current, $G_a(s)$ is the inverter equivalent transfer function, and $G_b(s)$ is the controlled object.

Since the inverter has the characteristics of high gain and small inertia, which transfer function can be expressed as follows:

$$G_a(s) = \frac{K_{\mathrm{SVPWM}}}{T_i s + 1} \tag{34}$$

In equation (34), T_i is the switching cycle of the inverter. Since the switching frequency of the inverter is much higher than the grid frequency, therefore $T_i s + 1 \approx 1$, the inverter link can be equivalent to a proportional gain link approximately, namely:

$$G_a(s) = K_{\mathrm{SVPWM}} \tag{35}$$

If the output current of the inverter is i_L, then:

$$L\frac{di_L}{dt} = u_{dc} - i_L R - u_s \tag{36}$$

In equation (36), R is the equivalent total resistance of the line, and the Laplace transform can be obtained by equation (36):

$$I_L(s) = \frac{U_{dc}(s) - U_s(s)}{Ls + R} \tag{37}$$

So the transfer function of the control object can be expressed as:

$$G_b(s) = \frac{1}{Ls + R} \tag{38}$$

B. DESIGN OF VOLTAGE LOOP STRUCTURE IN ENERGY STORAGE GRID-CONNECTED INVERTER SYSTEM

When the output power of the super capacitor energy storage system deviates from the output power of the inverter, a voltage is bound to be generated on the DC bus side. This voltage cannot be too large or too small, and the magnitude of the DC-side bus voltage reflects the equilibrium state of the input power of the energy storage grid-connected system to a certain extent. Therefore, the control of the bus voltage on the DC side is essential to ensure the stability of the entire system. The control of the voltage loop is used to realize the stable output mainly of the DC-side bus voltage. In view of the superior performance of LADRC, this article will introduce the improved LADRC technology to the voltage outer loop to maintain the stability of the DC-side bus voltage.

The dynamic characteristics of the voltage loop can be expressed as the following function:

$$C\frac{du_{dc}}{dt} = i_s \tag{39}$$

In equation (39), i_s is the current output from the energy storage system. Laplace transform of equation (40) gives:

$$U_{dc}(s) = \frac{I_s(s)}{Cs} \tag{40}$$

C. DESIGN OF DOUBLE-LOOP CONTROLLER STRUCTURE IN ENERGY STORAGE GRID-CONNECTED INVERTER SYSTEM

In the improved LADRC design of voltage loop, u_{dc} is the input signal of LADRC, i_d is the control input, that is, the reference input i_{q-ref}, u_{dc} and i_d of inner loop current can be obtained through measurement, so the improved LADRC combined with energy storage grid-connected inverter system can be designed as follows:

$$\begin{cases} z_1 = \dfrac{\left(\omega_0^2 T_\alpha + 2\omega_0\right)s + \omega_0^2}{s^2 + \left(\omega_0^2 T_\alpha + 2\omega_0\right)s + \omega_0^2}u_{dc} \\ \quad + \dfrac{}{s^2 + \left(\omega_0^2 T_\alpha + 2\omega_0\right)s + \omega_0^2}b_0 i_d \\ z_2 = \dfrac{\omega_0^2 T_\alpha s^2 + \omega_0^2 s}{s^2 + \left(\omega_0^2 T_\alpha + 2\omega_0\right)s + \omega_0^2}u_{dc} \\ \quad - \dfrac{\omega_0^2 T_\alpha s + \omega_0^2}{s^2 + \left(\omega_0^2 T_\alpha + 2\omega_0\right)s + \omega_0^2}b_0 i_d \\ z_3 = \dfrac{1}{\alpha T_\alpha s + 1}\dfrac{\omega_0^2 T_\alpha s^2 + \omega_0^2 s}{s^2 + \left(\omega_0^2 T_\alpha + 2\omega_0\right)s + \omega_0^2}u_{dc} \\ \quad - \dfrac{1}{\alpha T_\alpha s + 1}\dfrac{\omega_0^2 T_\alpha s + \omega_0^2}{s^2 + \left(\omega_0^2 T_\alpha + 2\omega_0\right)s + \omega_0^2}b_0 i_d \end{cases} \tag{41}$$

The linear control rate of the energy storage system can be designed as:

$$\begin{cases} i_{d0} = k_p\left(u_{ref} - u_{dc}\right) \\ u = \left(-z_3 + i_{d0}\right)/b_0 \end{cases} \tag{42}$$

Specific control principle: First, the DC bus voltage u_{ref} corresponding to the maximum power output of the super capacitor energy storage system is compared with the actual DC bus voltage u_{dc}. The error signal is processed by improved LADRC to obtain the reference input current i_{q-ref}, i_s compared with the actual output current, the error signal is superimposed on the actual voltage of the power grid after being processed by the PI controller, and the superimposed signal undergoes space vector pulse width modulation (SVPWM) to generate the modulation signal, thereby realizing the control of the inverter. The schematic diagram of two-stage super capacitor energy storage grid-connected control based on improved LADRC technology is shown in the following Fig. 13:

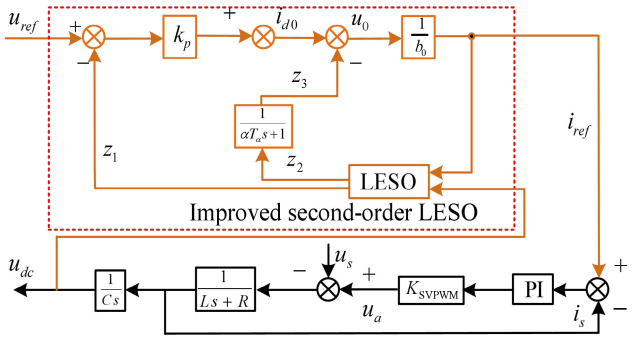

FIGURE 13. Schematic diagram of two-stage super capacitor energy storage grid-connected control with improved active disturbance rejection control.

VI. SIMULATION ANALYSIS

In order to verify the effectiveness of a new type of double closed-loop control strategy designed in this paper, a simulation model of 0.3MW grid-connected super capacitor energy storage system was established in MATLAB / Simulink, and then different working conditions were designed to perform digital simulation for theoretical analysis verification. Because the core of the double closed-loop controller designed in this paper is that the outer loop voltage loop has been optimized and improved, and the improved LADRC is used for control, while the inner loop current loop is still the traditional PI control, so it is aimed at the simulation verification the control effects of the outer loop are compared to prove the effectiveness of the improved voltage outer loop control strategy mainly. The main parameters of the 0.3MW super capacitor energy storage system on the grid-side are shown in APPENDIX A, and the controller parameters are shown in APPENDIX B.

In practical engineering applications, the energy storage system will be affected by grid-side voltage fluctuations when

it is connected to the grid. To further verify the effectiveness of improving the control effect of LADRC voltage outer loop in this paper, so that the controller can be used normally in the actual energy storage grid-connected system. Aiming at two different control methods before and after the improvement of LADRC, the low-voltage ride-through faults of different kinds and different degrees on the grid-side of the energy storage system are designed to prove the effectiveness of the improved LADRC voltage outer loop for DC-side bus voltage control.

A. SIMULATION ANALYSIS OF SYMMETRICAL LOW-VOLTAGE RIDE -THROUGH 20%

Setting the grid-side voltage of the energy storage system to drop symmetrically by 20% due to the fault. The fault starts at t = 0.5s and ends at t = 0.8s. The voltage waveform at the grid connection point is shown in Fig. 14a. Other conditions are the same, the dynamic response waveform of the DC-side bus voltage under the control of the LADRC control before and after the improvement is dropped symmetrically by 20% at the grid-side voltage, as shown in Fig 14b. Fig. 14c is the enlarged DC bus voltage waveform of Fig. 14b. The magnitude of the DC bus voltage fluctuation amplitude under two control modes and the rapidity of the voltage to reach a stable state after the fluctuation are selected as important reference indicators of control performance to analyze the effectiveness of improving the control effect of LADRC.

As can be seen from Fig. 14c, when the grid-side symmetrical low-voltage crosses 20%, the amplitude of the DC bus voltage fluctuation of the traditional LADRC control is large relatively, and the time to reach the system stable state is long relatively, indicating that the traditional LADRC controller is affected greatly by the grid-side voltage fault, and which the anti-interference performance is low relatively. The DC bus voltage fluctuation amplitude under the improved LADRC control is small relatively, which can quickly reach a stable state and show that the improved LADRC controller is less affected by grid-side voltage faults and has higher anti-interference performance.

B. SIMULATION ANALYSIS OF ASYMMETRICAL LOW-VOLTAGE RIDE -THROUGH 20% ON GRID-SIDE

Setting the grid-connected side voltage to drop asymmetrically by 20% due to the fault. The fault starts at t = 0.5s and ends at t = 0.8s. The voltage waveform at the grid-connected point is shown in Fig. 15a.

It can be seen from Fig. 15c that when the grid-side asymmetric low-voltage crosses 20%, the amplitude of the DC-side bus voltage fluctuation under traditional LADRC control is large relatively, and which is not easy to reach the stable state of the system during the fault, while improving LADRC control the amplitude of the DC bus voltage fluctuation is smaller significantly, indicating that the improved LADRC has better anti-interference to grid-side voltage faults. During the fault, the bus voltage waveform on the DC side is always in an unbalanced state, which also shows

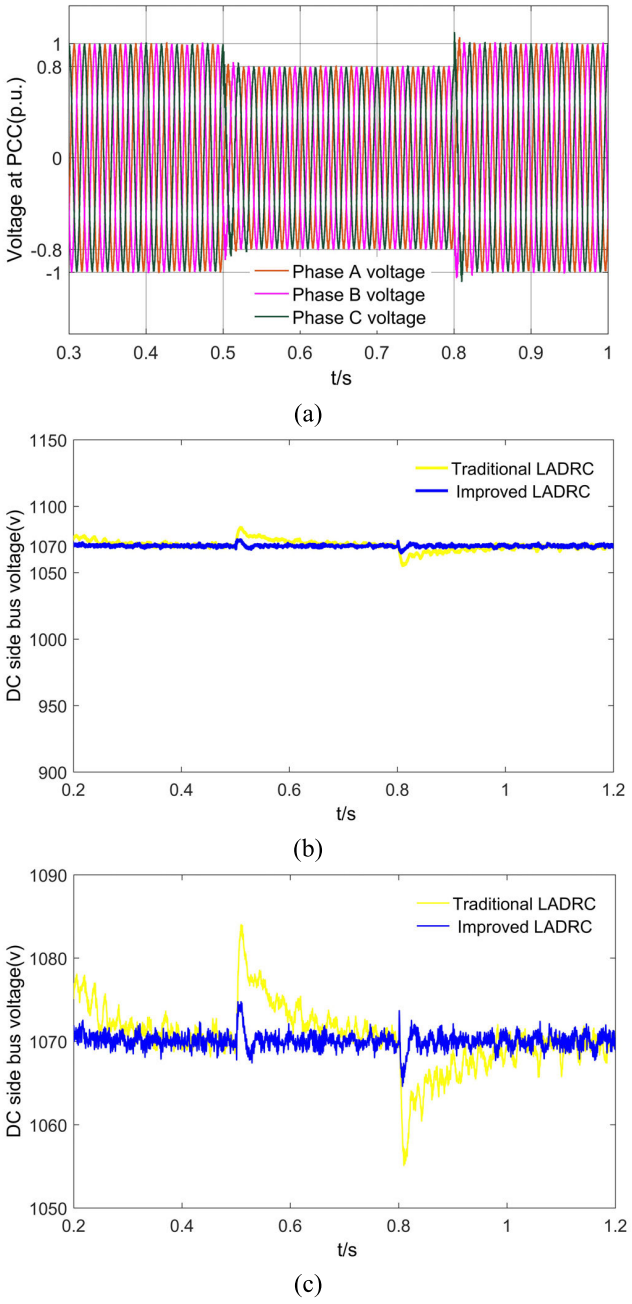

FIGURE 14. Voltage waveform of DC side bus under control of LADRC before and after improvement (a)Grid-connected point voltage waveform; (b) DC-side bus voltage waveform; (c) Enlarged view of DC-side bus voltage waveform.

that asymmetric faults have a greater impact on the system grid connection in actual projects. In general, no matter what kind of fault, the improved LADRC control has a better control effect on the stability of the DC bus voltage under the grid-side voltage fault.

C. SIMULATION ANALYSIS OF SYMMETRICAL LOW-VOLTAGE RIDE -THROUGH 40%

Setting the grid-connected side voltage to drop symmetrically by 40% due to the fault. The fault starts at t = 0.5s and ends

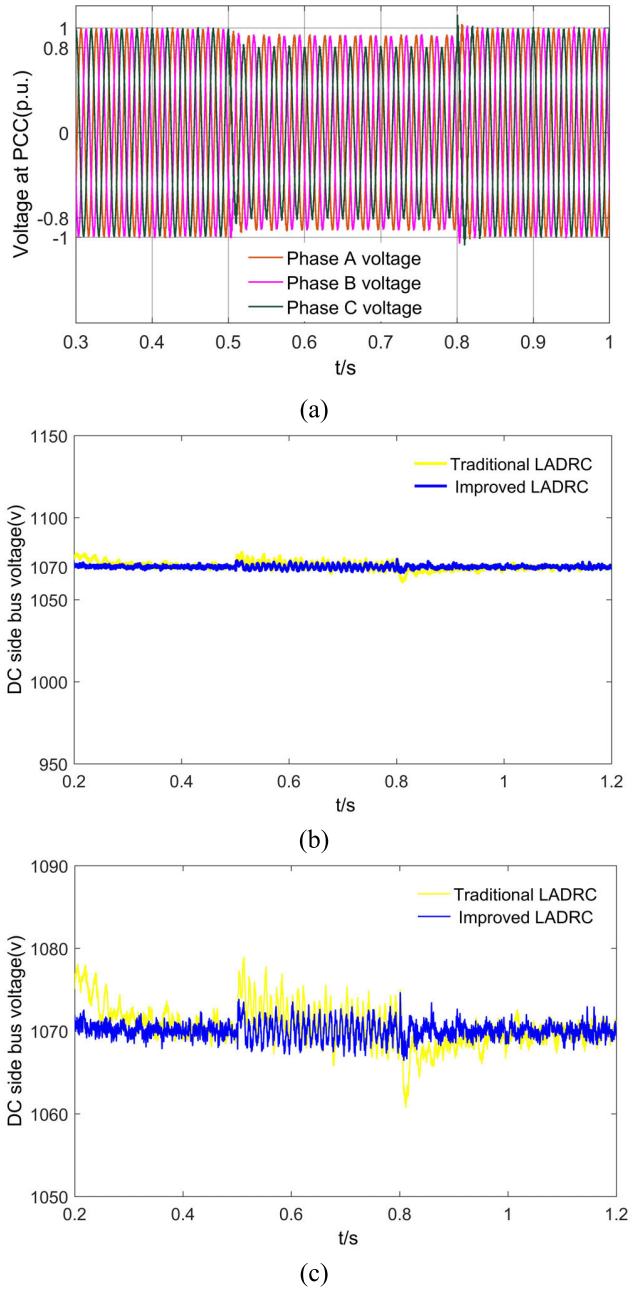

FIGURE 15. Voltage waveform of DC side bus under control of LADRC before and after improvement (a)Grid-connected point voltage waveform; (b) DC-side bus voltage waveform; (c) Enlarged view of DC-side bus voltage waveform.

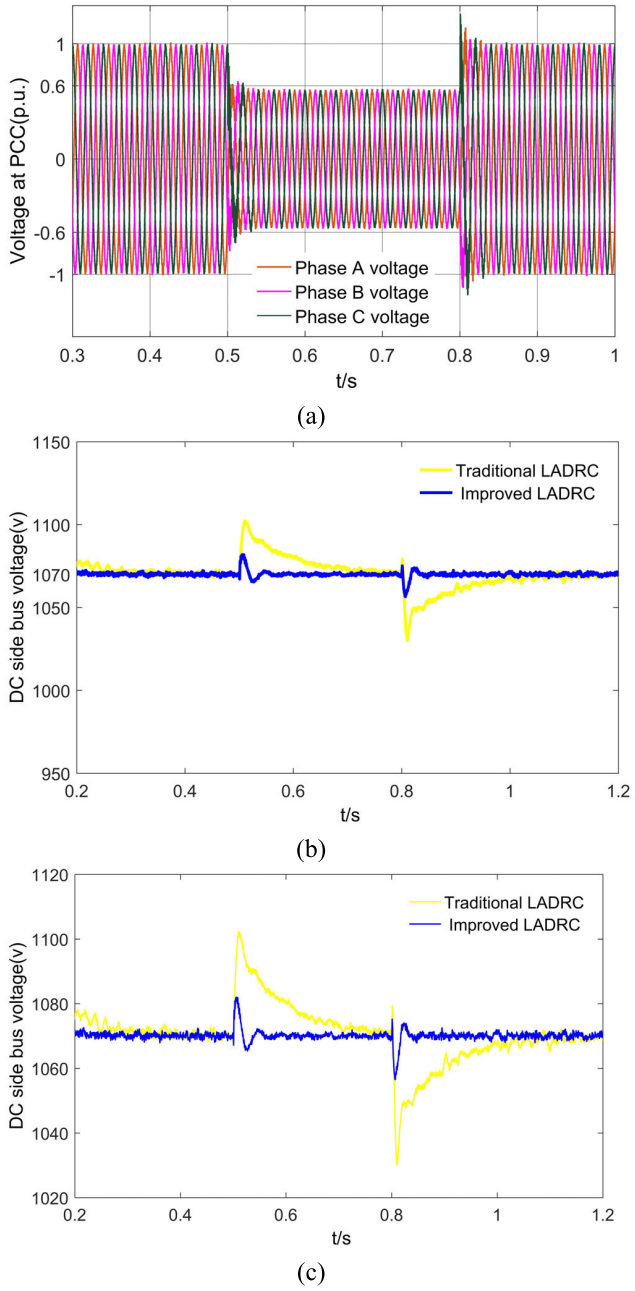

FIGURE 16. Voltage waveform of DC side bus under control of LADRC before and after improvement (a)Grid-connected point voltage waveform; (b) DC-side bus voltage waveform; (c) Enlarged view of DC-side bus voltage waveform.

at t = 0.8s. The voltage waveform at the grid-connected point is shown in Fig. 16a.

As can be seen from Fig. 16c, when the grid-side low-voltage drop 40% symmetrically, the amplitude of the DC-side bus voltage fluctuation under traditional LADRC control is large, and the time to reach the system stable state is long relatively, while the amplitude of the DC bus voltage fluctuation under the improved LADRC control is smaller significantly, and can reach a stable state quickly. Compared with the voltage drop 20% symmetrical on the grid-side, the fluctuation amplitude of the DC-side bus voltage becomes larger significantly, from which we can draw the following conclusion: the drop symmetrical of the grid-side voltage affects the magnitude of the DC-side bus voltage fluctuation amplitude, the greater the voltage drop, the greater the impact on the DC bus voltage.

D. SIMULATION ANALYSIS OF ASYMMETRICAL LOW-VOLTAGE RIDE -THROUGH 40% ON GRID-SIDE

Setting the grid-connected side voltage to drop 40% due to the fault asymmetry. The fault starts at t = 0.5s and ends

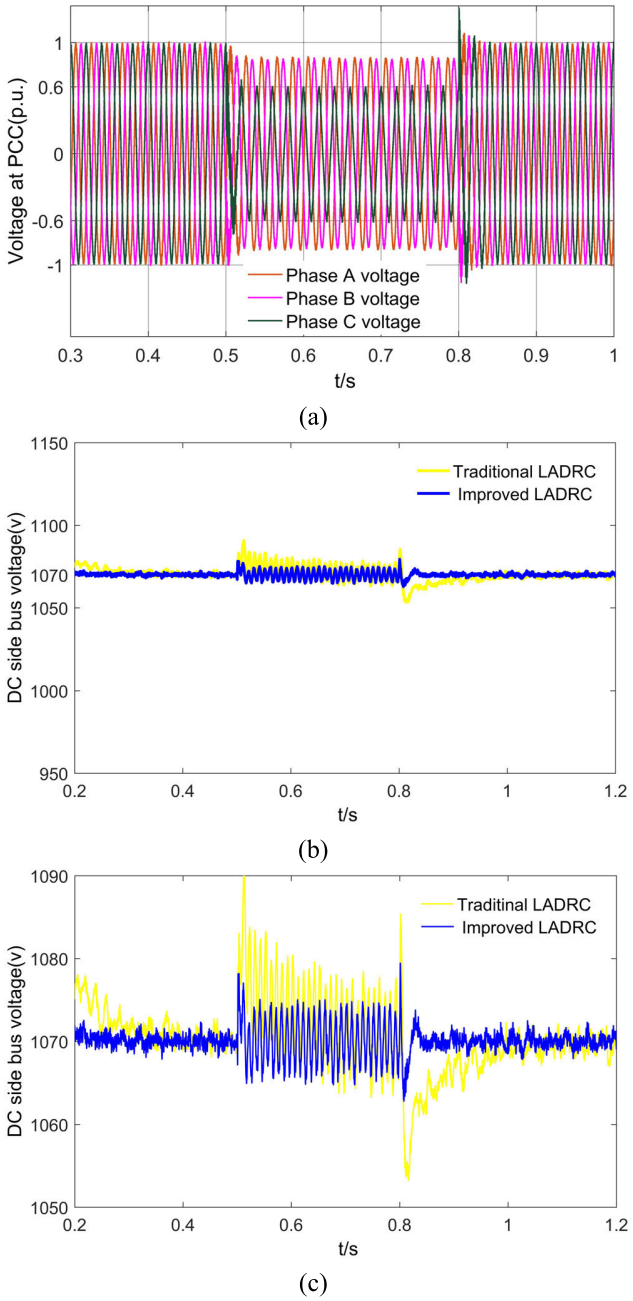

FIGURE 17. Voltage waveform of DC side bus under control of LADRC before and after improvement (a)Grid-connected point voltage waveform; (b) DC-side bus voltage waveform; (c) Enlarged view of DC-side bus voltage waveform.

at t = 0.8s. At this time, the grid-connected voltage waveform is shown in Fig. 17a.

It can be seen from Fig. 17c that when the grid-side low-voltage drop 40% asymmetrically, the amplitude of the DC bus voltage fluctuation of the traditional LADRC control is greater significantly than the amplitude of the DC bus voltage fluctuation under the improved LADRC control. Compared with the same type of grid-side asymmetric low- voltage ride-through 20%, the greater the asymmetry of the grid-side voltage, the greater the impact on the system DC-side bus voltage. Therefore, the improved LADRC control has a better control effect on the stability of the DC bus voltage under the condition of low-voltage asymmetric crossing, indicating that the improved LADRC has better anti-interference performance for the fault of the grid-side voltage.

VII. CONCLUSIONS

This paper takes the DC link bus voltage of the energy storage grid-connected inverter as the control target, and takes the energy storage grid-connected inverter as the control object. Based on the analysis of the working principle of the energy storage grid-connected system, in order to improve the performance of the traditional LADRC technology, on the basis of introducing the proportional differential link in the traditional LESO, to overcome the shortcomings of the serious phase lag of LESO and the problem of poor high-frequency noise suppression ability. According to the idea of correcting the system in the principle of automatic control to improve the performance of the system controller, an improved first-order LADRC with the output voltage and its differential as the state variable is proposed to replace the voltage outer loop control in the traditional double closed loop control to improve the anti-interference ability of LADRC technology. Secondly, introduce the differential term of the output voltage error in LESO, and add a first-order inertial link in the channel of the sum disturbance. Finally, through the analysis of the frequency response characteristics of the improved LADRC system, which can be seen that with the increase of frequency, the decrease in the amplitude of the disturbance observation is reduced effectively, and the observation bandwidth of the LESO is increased. The effect also improves the anti-disturbance capability of the LADRC.

In this paper, the simulation research and analysis of symmetric and asymmetric faults were carried out under the condition of setting low-voltage ride-through 20% and 40% on the grid-connected side of the super capacitor energy storage system. The results show that the improved LADRC control has a better control effect on the stability of the DC-side bus voltage under the grid-side voltage fault, which proves the effectiveness of the controller designed in this paper.

However, the research results of this article are only the most of the content of the subject research. In the following topic research, we will continue to deepen and study the two aspects of this paper. On the one hand, the core of this article is to add a lead lag correction link to the traditional LADRC technology, and introduce a first-order inertia link in the sum disturbance channel. Although the control performance of the controller is improved greatly, which also brings some difficulties to the parameter setting of the controller. Therefore, the following research work is focused on parameter setting mainly, such as the application of some artificial intelligence algorithms and LADRC to find an efficient and fast parameter setting method to meet the needs of actual engineering as much as possible. On the other hand, the working condition verification in this paper focuses on the condition of low-voltage penetration on the grid-side, and there are still some

limitations for the study of the condition of high-voltage penetration on the grid-side. Therefore, the verification of the controller designed in this paper under more actual working conditions is also part of the work of the next paper.

APPENDIX A

See Table 1.

TABLE 1. Parameters of Grid-connected Side of 0.3MW super capacitor energy storage system.

Symbol	Quantity	Value	Unit
p	Rated power	MW	0.3
V_g	Rated voltage	V	590
f	Rated Frequency	HZ	50
u_{dc}	DC-side bus voltage	V	1070
C	DC-side bus capacitor	μF	240
R	Grid-side filter resistance	Ω	0.942
C	Grid-side filter capacitor	μF	147
L	Grid-side filter inductance	mH	120

APPENDIX B

See Table 2.

TABLE 2. Controller parameters.

Symbol	Quantity	Value
ω_c	Controller bandwidth	3000
ω_0	Observer bandwidth	500
b_0	Control gain	20000

REFERENCES

[1] M. G. Molina, "Energy storage and power electronics technologies: A strong combination to empower the transformation to the smart grid," *Proc. IEEE*, vol. 105, no. 11, pp. 2191–2219, Nov. 2017.
[2] H. Nian, Y. Xu, L. Chen, and G. Li, "Frequency coupling characteristic modeling of grid-connected inverter and system stability analysis," *Proc. CSEE*, vol. 39, no. 6, pp. 1421–1431, Nov. 2019.
[3] Y. Liu, S. Niu, and W. Fu, "Design of an electrical continuously variable transmission based wind energy conversion system," *IEEE Trans. Ind. Electron.*, vol. 63, no. 11, pp. 6745–6755, Nov. 2016.
[4] X. Guo, W. Liu, and Z. Lu, "Flexible power regulation and current-limited control of the grid-connected inverter under unbalanced grid voltage faults," *IEEE Trans. Ind. Electron.*, vol. 64, no. 9, pp. 7425–7432, Sep. 2017.
[5] J.-S. Lee, K.-B. Lee, and F. Blaabjerg, "Predictive control with discrete space-vector modulation of Vienna rectifier for driving PMSG of wind turbine systems," *IEEE Trans. Power Electron.*, vol. 34, no. 12, pp. 12368–12383, Dec. 2019.
[6] A. Rodriguez-Cabero, M. Prodanovic, and J. Roldan-Perez, "Full-state feedback control of Back-to-Back converters based on differential and common power concepts," *IEEE Trans. Ind. Electron.*, vol. 66, no. 11, pp. 9045–9055, Nov. 2019.
[7] J. Han, "From PID to active disturbance rejection control," *IEEE Trans. Ind. Electron.*, vol. 56, no. 3, pp. 900–906, Mar. 2009.
[8] J. Liu, S. Vazquez, L. Wu, A. Marquez, H. Gao, and L. G. Franquelo, "Extended state observer-based sliding-mode control for three-phase power converters," *IEEE Trans. Ind. Electron.*, vol. 64, no. 1, pp. 22–31, Jan. 2017.
[9] G. Wang, R. Liu, N. Zhao, D. Ding, and D. Xu, "Enhanced linear ADRC strategy for HF pulse voltage signal injection-based sensorless IPMSM drives," *IEEE Trans. Power Electron.*, vol. 34, no. 1, pp. 514–525, Jan. 2019.
[10] S. Ding, W.-H. Chen, K. Q. Mei, and D. J. Murray-Smith, "Disturbance observer design for nonlinear systems represented by input–output models," *IEEE Trans. Ind. Electron.*, vol. 67, no. 2, pp. 1222–1232, Feb. 2020, doi: 10.1109/TIE.2019.2898585.
[11] C. Du, Z. Yin, J. Liu, Y. Zhang, and X. Sun, "A speed estimation method for induction motors based on active disturbance rejection observer," *IEEE Trans. Power Electron.*, vol. 35, no. 8, pp. 8429–8442, Aug. 2020, doi: 10.1109/TPEL.2020.2964573.
[12] Z.-Q. Chen, M.-W. Sun, and R.-G. Yang, "On the stability of linear active disturbance rejection control," *Acta Automatica Sinica*, vol. 39, no. 5, pp. 574–580, Dec. 2013.
[13] Y. Wu, B. Jiang, and N. Lu, "A descriptor system approach for estimation of incipient faults with application to high-speed railway traction devices," *IEEE Trans. Syst., Man, Cybern. Syst.*, vol. 49, no. 10, pp. 2108–2118, Oct. 2019.
[14] Y. K. Wu, B. Jiang, and Y. L. Wang, "Incipient winding fault detection and diagnosis for squirrel-cage induction motors equipped on CRH trains," *ISA Trans.*, vol. 99, p. 488 495, Sep. 2020.
[15] A. S. Hadi, M. S. Shaker, and Q. A. Jawad, "Estimation/decoupling approach for robust Takagi–Sugeno UIO-based fault reconstruction in nonlinear systems affected by a simultaneous time-varying actuator and sensor faults," *Int. J. Syst. Sci.*, vol. 50, no. 13, pp. 2473–2485, Oct. 2019, doi: 10.1080/00207721.2019.1671528.
[16] Z. Gao, "Scaling and bandwidth-parameterization based controller tuning," in *Proc. Amer. Control Conf.*, Denver, CO, USA, Jun. 2003, pp. 4989–4996.
[17] J. Li, X. Qi, Y. Xia, and Z. Gao, "On linear/nonlinear active disturbance rejection switching control," *Acta Autom. Sinica*, vol. 42, no. 2, pp. 202–212, Oct. 2016.
[18] J. Liu, W. Yao, J. Fang, J. Wen, and S. Cheng, "Stability analysis and energy storage-based solution of wind farm during low voltage ride through," *Int. J. Electr. Power Energy Syst.*, vol. 101, pp. 75–84, Oct. 2018.
[19] Y. X. Su, C. H. Zheng, and B. Y. Duan, "Automatic disturbances rejection controller for precise motion control of permanent-magnet synchronous motors," *IEEE Trans. Ind. Electron.*, vol. 52, no. 3, pp. 814–823, Jun. 2005.
[20] A. Krama, L. Zellouma, A. Benaissa, B. Rabhi, M. Bouzidi, and M. F. Benkhoris, "Design and experimental investigation of predictive direct power control of three-phase shunt active filter with space vector modulation using anti-windup PI controller optimized by PSO," *Arabian J. Sci. Eng.*, vol. 44, no. 8, pp. 6741–6755, Aug. 2019.
[21] D. Yuan, X.-J. Ma, Q.-H. Zeng, and X. Qiu, "Research on frequency-band characteristics and parameters configuration of linear active disturbance rejection control for second-order systems," *Control Theory Appl.*, vol. 30, no. 12, pp. 1630–1640, Dec. 2013.
[22] L. Yang, J. Zeng, W. Ma, and Z. Huang, "Voltage control of microgrid inverter based on improved second-order active disturbance rejection technology," *Power System. Autom*, vol. 43, no. 4, pp. 685–703, Feb. 2019.

YOUJIE MA received the bachelor's, master's, and Ph.D. degrees in power system and automation from Tsinghua University, in 1993. From 1993 to 2002, she has worked with the School of Electrical and Automation Engineering, Qingdao University, where she was promoted to a Full Professor, in 1998. Since 2002, she has been working with the School of Automation, Tianjin University of Technology.

LUYONG YANG is currently pursuing the master's degree with the School of Electrical and Electronic Engineering, Tianjin University of Technology, Tianjin, China.

His research interest includes grid-connected control of new energy power generation systems.

XUESONG ZHOU received the bachelor's degree in electrical engineering from the South China University of Technology, Guangzhou, China, in 1984, and the master's and Ph.D. degrees in electrical engineering from Tsinghua University, in 1990 and 1993, respectively.

From 1993 to 2002, he was the Deputy Dean of the School of Electrical and Automation Engineering, Qingdao University. He joined the Tianjin University of Technology as a Professor, in 2002. His research interest includes development and use of power electronics and renewable energy.

XIA YANG was born in Hebei, China, in 1994. She is currently pursuing the master's degree with the School of Electrical and Electronic Engineering, Tianjin University of Technology, Tianjin, China.

Her research interest includes grid-connected control of wind power systems and harmonics in new energy systems.